

Haizhen Sun, Terry L. Clark, Roland B. Stull and Andy T. Black
University of British Columbia, Vancouver, British Columbia, Canada

1. INTRODUCTION

Net ecosystem-atmosphere exchange (NEE) of carbon dioxide is controlled in part by many factors including atmospheric turbulence and advection. Vertical turbulent fluxes of carbon dioxide are measured by eddy correlation (EC) instruments, however, mean horizontal and vertical advection effects on NEE may be significant in complex (coastal, mountainous) terrain (Lee, 1998; Yi et al., 2000; Staebler and Fitzjarrald, 2003; Eugster and Siegrist, 2000; Morgenstern et al., 2004), but are more difficult to measure or estimate.

The West Coast Flux tower site is located on a 5-10 degree slope oriented east/northeast on Vancouver Island, where katabatic and anabatic winds induced by differential heating and cooling are expected to be strong during fair weather (Stull, 1988). Therefore understanding wind and turbulent regimes is important and also a prerequisite for more meaningful interpretations of NEE estimates from the West Coast Flux tower data. Furthermore the measurements of eddy flux (vertical turbulent fluxes) at the West Coast Flux tower site are anomalous just after sunset during fair weather (see figure 1); this behavior is as yet poorly understood.

Therefore the first goal of the study is to investigate the influence of the canopy elements on the dynamics and thermodynamics of canopy flow over complex terrain, the second goal is to assess the strengths and weaknesses of current procedures used to estimate NEE at the West Coast Flux station. To achieve these two goals the high-resolution mesoscale weather model developed by Clark (1977, 1979) is further refined to treat tree drag and canopy radiation effects in the study.

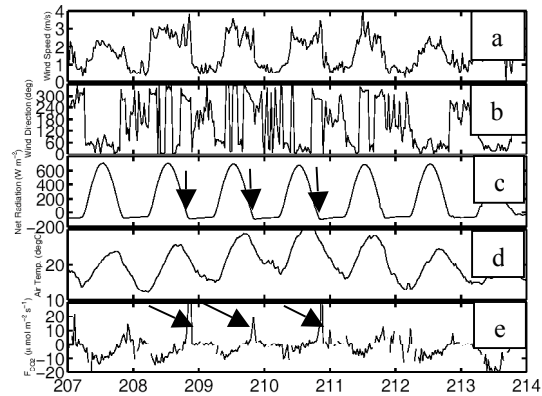


Figure 1. Time series of measurements of wind speed (a), wind direction (b), net radiation (c), air temperature (d), CO_2 eddy flux (e) at the main tower site of West Coast Flux station on Vancouver Island during days 207-214, 2003. (Data came from the UBC Biometeorology/Soil Physics Group)

2. Methodology

2.1 Numerical model

The anelastic, non-hydrostatic mesoscale model developed by Clark (1977, 1979) uses vertically stretched terrain following coordinates with horizontal and vertical interactive grid refinement (Clark and Farley, 1984; Clark and Hall, 1991, 1996). With the recent developments of Message Passing Interface (MPI) and fire dynamics (Clark et al., 2003), the model has become known as WFIS.

The model has been widely used to study deep convective cloud simulations (Lane et al., 2003); airflow over complex terrain and severe down-slope wind storms (Clark and Farley, 1984); clear air turbulence (Clark, 2000); and since about 1994, wildfires (Clark et al., 2003).

As part of this project we included both canopy dynamics and thermodynamics and a conservation equation for CO_2 in the WFIS code. The parameterizations of the CO_2 source/sink terms are still under evaluation.

* Corresponding author address: Haizhen Sun, University of British Columbia, Dept. of Earth and Ocean Sciences, 6339 Stores Road, Vancouver, BC V6T 1N4, Canada; e-mail: hsun@eos.ubc.ca

2.2 Treatment of canopy drag

For canopy drag we followed Wilson et al. (1998) and treated the drag as

$$F_i(z) = \square Cn_d a(z) |\vec{V}| u_i \quad (1)$$

where $|\vec{V}|$ is the amplitude of the wind speed, Cn_d the canopy drag coefficient, and $a(z)$ is the needle (or leaf) area density (the one-sided leaf area per unit volume) in units of m^2/m^3 . Data from the UBC Biome/soil group for the West Coast Flux station project is used to specify the Leaf Area Index (LAI), $a(z)$, as:

$$a(z) = \frac{7}{5} \left(1 - \frac{z - 23}{10}\right) \quad \text{for } 23 < z < 33 \quad (2)$$

so that the cumulative leaf area index (the vertical integration of $a(z)$) is 7 from the canopy base (23 m) to canopy top (33 m), i.e.

$$LAI = \int_{23}^{33} a(z) dz = 7 \quad (3)$$

The vertical leaf area density distribution is shown in Figure 2.

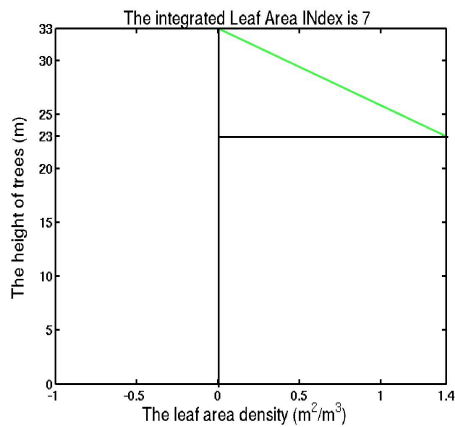


Fig. 2 Vertical distribution of leaf area density (m^2/m^3). Vertical integration produces leaf area index (LAI) of 7.

It is difficult to measure the effective drag coefficient for a forest canopy due to problems of the shelter effect (Thom, 1971) and leaf orientation. The effective Cn_d of a single leaf measured in wind tunnel changes with the leaf

orientation and turbulent scales and intensity around the leaf (Raupach and Thom, 1981). Wilson et al. (1998) suggest using $Cn_d = 1$, which is a rather large value in terms of an adjustment time. Shaw et al. (1988) use an isotropic drag coefficient and let $Cn_d = 0.15$,

which is the value used in this study. Thus Cn_d in the first case was used as an adjustable model parameter and in the second as a data input. This points to a major weakness in our understanding of canopy flows where we cannot predict the drag on the foliage from knowledge of the canopy geometry and the behavior of the plant elements in isolation.

2.3 Energy budget within the canopy

The major components of the conservation of energy within the canopy is given by:

$$R_{NP} = H + LE + S_t + P_s \quad (4)$$

The effect of canopy elements on the energy budget within the canopy layer and surface layer are treated similar to Yamada (1982). The net radiation R_{Nh} at treetop ($z = h$) is given by:

$$R_{Nh} = (1 - \square_t) S + R_{Lh\square} - R_{Lh\uparrow} \quad (5)$$

where \square_t is the canopy albedo, S is the direct solar radiation, $R_{Lh\square}$ and $R_{Lh\uparrow}$ are the incoming and outgoing long-wave radiation, respectively, and are calculated using the detailed scheme in Redelsperger and Clark (1991).

The net radiation within the canopy R_{Np} follows Uchijima (1961), quoted in Ross (1975):

$$R_{Np}(z) = R_{Nh} \left[\exp\{-\square k a(z)\} - \square \square \left(1 - \frac{z}{h}\right) \exp\{-\square k a(0)\} \right] \quad (6)$$

where \square is the fraction of area covered with trees, $a(z)$ is the leaf area in a volume at height z , k denotes an extinction coefficient, R_{Nh} is calculated with Eqn. (5), and h is the canopy height. The second term in parenthesis on the right hand side of Eqn. (6) is added to insure that the net radiation vanishes at the ground when the surface is completely covered with trees ($\square = 1$).

The storage of heat within the canopy is treated by assuming the canopy and air are at the same

temperature. Energy used in photosynthesis is neglected and the heat budget within a canopy is given by

$$\frac{\partial \theta}{\partial t} = \frac{(1 - \alpha) \partial R_N}{\rho_0 C_p \partial z} + \frac{\theta}{\rho_0 C_p + \rho_c C_c} \left(1 + \frac{1}{B}\right) \frac{\partial R_{NP}}{\partial z} \quad (7)$$

where the Bowen Ratio B ($=H/LE$) in a canopy is assumed to be constant with height, ρ_0 and ρ_c is the air density and canopy density, respectively, C_p and C_c is the heat capacity of air and canopy, respectively, C_c/C_p is set to 0.65 in the model, α is the fraction of area covered with trees, $\alpha=1$ represents a dense forest, and $\alpha=0$ bare soil.

2.4 Surface heat budget

The surface energy balance is treated as Devonec and Barros (2002):

$$c^* h_0 \frac{\partial T_0}{\partial t} = F_R + S_h + L_h + G_h \quad (8)$$

the left-hand term of eqn. (8) is the change in heat storage in the superficial soil layer, C^* is the volumetric heat capacity of the land surface, T_0 is the temperature of soil superficial layer, h_0 is the depth of superficial soil layer ($=0.12\text{m}$). F_R is the total radiative flux comprising net shortwave and net long-wave radiation, S_h and L_h are the sensible and latent heat flux between the surface and the atmosphere, G_h is conduction into or out of the sub-medium (soil or water).

Considering the canopy shadowing effect on net radiation budget of surface, F_R in eqn. (8) is give as:

$$F_R = (1 - \alpha) [(1 - \alpha) S + \alpha (R_{LG\downarrow} - R_{LG\uparrow})] \quad (9)$$

where α is the surface albedo, $R_{LG\downarrow}$ is the incoming long-wave radiation, $R_{LG\uparrow}$ is the outgoing long-wave radiation. α is the IR emissivity of the ground.

In eqn.(8), the sensible heat flux S_h and latent heat flux L_h between the ground and the adjacent air are expressed as Devonec and Barros, (2002):

$$S_h = C_p \alpha K_H |U_1| (T_1 - T_0) \quad (10)$$

$$L_h = L_v \alpha K_w |U_1| (q_1 - q_{sat}) \quad (11)$$

The subscript 1 denotes the reference height in the boundary layer at which the horizontal wind U_1 , the temperature T_1 , and the specific humidity q_1 are taken. We use values at the first layer above the ground. K_H and K_w are the aerodynamic drag coefficient for heat and water vapor transfer, respectively, and assumed equal. q_{sat} is the saturated specific humidity at the ground surface. L_v is the latent heating rate for water vaporization, and C_p is the heat capacity of the air at constant pressure.

2.5 Carbon dioxide budget

The conservation equation of carbon dioxide will be used to numerically quantify the various contributions. We will assess the contributions due to horizontal (parallel to the slope) advection versus actual source/sink and vertical diffusion effects, and also assess the effects of temporal and spatial filtering on the NEE estimates at the West Coast Flux station.

3. Numerical experiments

A series of numerical experiments are performed to investigate the effects of tree drag, the topography as well as the diurnal cycle on canopy flow. All these numerical experiments are performed using two-dimensional (2D) applications of the WFIS model. Such two-dimensional calculations are useful for understanding the complex effects of tall trees on air circulation in the boundary layer. They provide theoretical and physical guidance for more computationally intensive three-dimensional calculations. Also in two dimensions higher resolutions can be attained in comparison to three-dimensional (3D) calculations. The model is 2D in the y-direction that we take as running from west to east. Due to space limitations, we describe only some diurnal cycle response experiments.

3.1 Initial condition

The topography is an idealization of the mountains to the west of Campbell River. The atmosphere is taken as very weakly stable (Brunt-Vaisala frequency, $N=0.001 \text{ s}^{-1}$) from $z=0$ to 2 km for the boundary layer. The free

atmosphere uses $N=0.01 \text{ s}^{-1}$ from $z = 2$ to 13.5 km. The stratosphere assumes $N=0.02 \text{ s}^{-1}$ above 13.5 km. Zero ambient wind is described for all height, Coriolis force is off for these experiments. At $z=0$ a surface temperature of 300K for the land and 288 K for the water was specified.

Over land the surface stress (with or without tree-drag) is taken as

$$\tau_{23}|_{z=sfc} = C_d |V| v \quad (12)$$

With $C_d=0.04$. Over the water we put $\tau_{23}=0$.

The eddy-mixing coefficient for internal flow above the surface uses the first order closure of Smagorinsky (1963) and Lilly (1962).

3.2 Experimental design

The experiment geometry is described in Table 1. The domain specification for these experiments is shown in figure 3. The size of outer domain is 86.4 km from western to eastern side, a canopy of trees 33 m high and 1300 m topography is specified from 11.25 km to 63.95 km, the ocean is from 0 km to 11.25 km and from 63.95 km to 86.4 km. The length scale and topography is similar to that of Vancouver Island. The nested domain is on the eastern side of the mountain (island).

The dynamics is turned off for Th1 experiment and the simulation is run for 100 hours starting at $10:00$ am LST. These simulations assume solar radiation in late July (July 30th). The purpose for this experiment is to test the energy budget code.

Exp Th2 is the same as Th1 except the dynamics is active. This experiment runs for 48 hours starting at 10 am local time. We use $Cn_d = 0.15$ (Amiro,1990). This experiment shows the basic diurnal and terrain response of canopy flow.

These two experiments use the same initial conditions and canopy cover, $L_f = 1.0$.

Table 1. Description of experiments. Dy and Dz represent the horizontal and vertical grid size, respectively. Dt is time step. Dyna means dynamics and NVL the number of nests.

Exp.	Dy (m)	Dz (m)	Dt (s)	Dyna	NVL
Th1	150/75	12/6	30./15.	Off	2
Th2	150/75	12/6	3.75/1.875	On	2

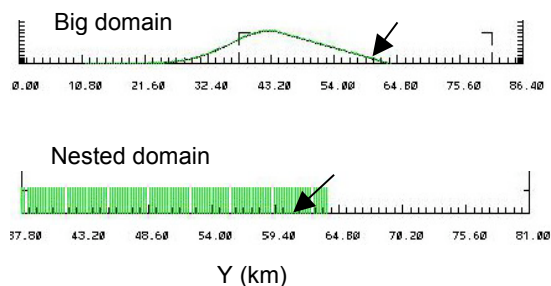


Figure 3. The topography and canopy specification. The green color represents the area covered by the canopy. The nested domain is located on the eastern side of the mountain. The location pointed by arrows is the position for analysis shown in fig. 4 and fig. 5.

3.3 Results

a. Column energy budget analysis

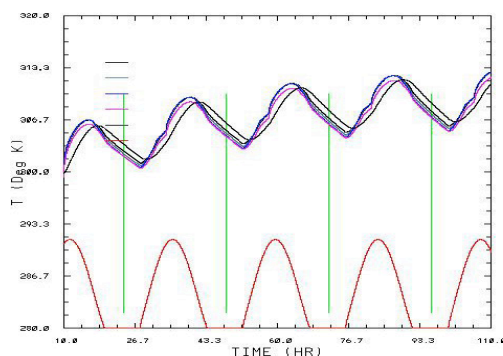


Figure 4 . Column energy budget simulation for Th1 experiment. The red lines at bottom indicate solar radiation cycle and the lagged black line above shows surface temperature of the ground. The other four solid lines show the air temperature at the first 4 vertical grid points above the surface.

Figure 4 shows a four-day diurnal cycle simulation for experiment Th1 at a single horizontal point (grid 405, at domain 60.67 km) in the model, which is indicated by arrows in fig 3. This calculation is representative of conditions under and within a mature 33 m high canopy. The high LAI ($=7$), which represents very dense forest at the West Coast Flux tower site, results in very small vertical air temperature differences throughout the canopy with a diurnal temperature range of approximately 9 deg K. This temperature range is even smaller than the approximately 7 deg K for the soil superficial layer (at the depth of 12 cm). The results show good agreement with Yamada (1982).

With the dense canopy and advection turned off, heat accumulates within the canopy, the air and soil temperature show increasing tendency for the four-day simulation, which show a good

agreement with the observations in Fig.1(d). It also is evident that the variation of soil temperature lags the air temperature.

Figure 5 shows a 2 day diurnal cycle simulation for Th2 experiment with the dynamics turned on. The difference in the temperature range is much smaller for Th2 compared with Th1. It is about 5 deg K and with no increasing tendency. The eddy mixing and advective transport are the main reasons for these differences.

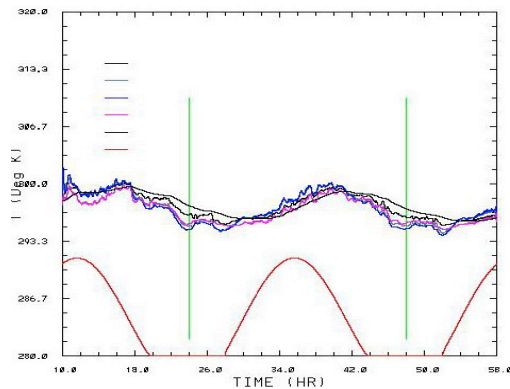


Figure 5. Same as fig.4 but for Exp. Th2 with the dynamics turned on.

b. Wind structure

Figure 6 shows the horizontal winds, v , at four times spaced 6 hours apart for diurnal two-dimensional flow over Vancouver Island for experiment Th2. The daytime convective upslope and nighttime stable downslope flows are evident. One interesting result is the seemingly good agreement of the switch from upslope to down-slope flow that occurs shortly after sunset on the eastern slope at $t=1900$, which shows the complex nature of the wind pattern change.

The dynamical explanation for this behavior is quite clear from the results, namely a combination of west-slope dominant upslope winds extending over the ridge near sunset because of the stronger heating rates on that slope. The elimination of sensible heating on the eastern slope then allows a very quick transition to down-slope winds over the entire eastern slope in about one hour after sunset. This is considered important to understanding some of the CO_2 anomalous measurements just after sunset at the FLUX site.

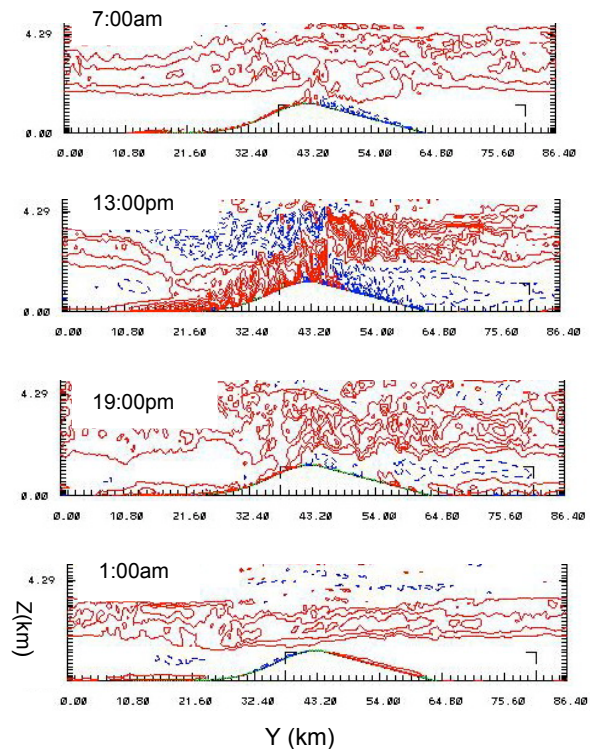


Figure 6. Horizontal wind at the four times of 07, 13, 19 and 01 hrs local time showing diurnal response for the outer nest for Th2. Contour interval is 1 m/s with solid (red) showing positive values from west to east and dashed (blue) showing negative.

Figure 7 shows the statistics for the maximum vertical (a) and horizontal (b) velocity for experiment Th2. The wind speeds also show a diurnal cycle. The range of maximum velocity is 1~14 m/s. The maximum velocity amplitudes occur between 2 and 3 pm local time during daytime strong convection. The nocturnal amplitudes are small and nearly constant, especially for vertical velocity, which is in agreement with the small turbulence flux measurements at the tower site on calm nights (Morgenstern et al. 2004).

C. Thermal structures

Figure 8 shows the thermal structure for the inner domain for experiment Th2. We denote the topography above the frame. In fig. 8b the wind vectors over the land show that the strong updrafts correspond to strong thermal convection near 13:00 pm and a sea breeze pattern is evident. Very light winds are shown at night (fig.8a) below 200 m indicating a relatively stable boundary, but within the canopy the air is

still warmer than that above. The ocean is warmer than the land at night causing a warm tongue to extend from the water surface onto the neighboring canopy. A weak land breeze also can be seen in Fig. 8 a.

4. Conclusion

The WFIS model has been developed to include the canopy drag dynamics and the effect of canopy elements on canopy and surface energy budget. Diurnal variation of all variables is computed by taking the canopy radiation balance into consideration, the diurnal cycle simulation experiments capture the first-order effects of diurnal heating/cooling on the sloping terrain and heterogeneous roughness surface.

The 2D experiments appear to be quite useful for understanding the complex effects of tall trees on the air circulation in the boundary layer. The volume exchange of heat and momentum above and within the canopy located on a hill appear to be strongly affected by the local flows resulting from diurnal thermal forcing which may help explain the anomalous measurements just after sunset.

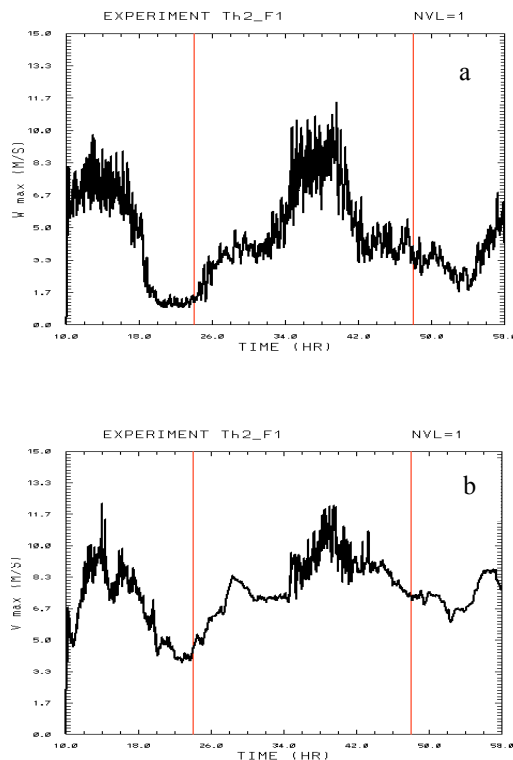


Figure 7. The maximum vertical (a) and horizontal velocity (b) versus model running time for the outer domain. The red line indicates midnight.

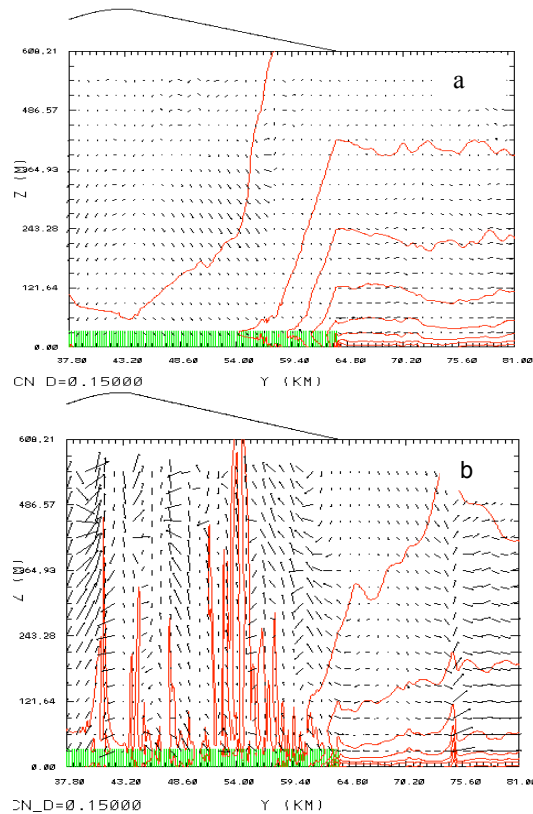


Figure 8. Potential temperature (\square) for the inner domain for Exp Th2 at 1:00 am (a) and 13:00 pm (b) LST as well as the correspond wind vectors (black arrows).

Reference

Amiro, B.D., 1990: Drag coefficients and turbulence spectra within three boreal forest canopies. *Boundary-Layer Meteor.* **52**, 227-246

Clark, T. L., 1977: A small-scale dynamic model using a terrain-following coordinate transformation. *J. Comp. Phys.* **24**: 186-215

\square , 1979: Numerical simulations with a three-dimensional cloud model: Lateral boundary condition experiments and multicellular severe storm simulations. *J. Atmos. Sci.* **36**: 2192-2215

\square , and Farley, W.R., 1984: Severe downslope windstorm calculations in two and three spatial dimensions using anelastic interactive grid nesting: A possible

- mechanism for gustiness. *J. Atmos. Sci.* **41**: 329-350
- , and Hall, W.D., 1991: Multi-domain simulations of the time dependent Navier Stokes equation: Benchmark Error analyses of nesting procedures. *J. Comp. Phys.* **92**, 456-481
- , and Hall, W.D., 1996: On the design of smooth, conservative vertical grids for interactive grid nesting with stretching. *J. Appl. Meteor.* **35**, 1040-1046.
- , and Hall, W.D., Kerr, R.M., Middleton, D., Radke, L., Ralph, F.M., Neiman, P.J., and Levinson, D., 2000: Origins of aircraft-damage clear-air turbulence during the 9 December 1992 Colorado downslope windstorm: Numerical simulations and comparison with observations. *J. Atmos. Sci.* **57**, 1105-1131
- , Griffiths M., Reeder, M.J., Latham, D., 2003: Numerical simulations of grassland fires in the Northern Territory, Australia: A new subgrid-scale fire parameterization. *J. Geo. Res.* **108**, 1-15.
- Devonec, E. and Barros, A.P., 2002: Exploring the transferability of a land-surface hydrology model. *J. Hydro.* **265**, 258-282.
- Eugster, W. and Siegrist, F., 2000: The influence of nocturnal CO₂ advection on CO₂ flux measurements. *Basic Appl. Ecol.* **1**, 177-188.
- Lane, T.P., Sharman, R.D., Clark, L.T., and Hsu, H.M., 2003: An investigation of turbulence generation mechanisms above deep convection. *J. Atmos. Sci.* **60**: 1297-1321.
- Lee, X. 1998: On micrometeorological observations of surface-air exchange over tall vegetation. *Agricultural and Forest Meteorology*, **91**: 39-49.
- Lilly, D.K., 1962: On the numerical simulation of buoyant convection. *Tellus*, **14**: 145- 172.
- Morgenstern, K., Black, T.A., Humphreys, E.R., Griffis, T.J., Drewitt, G.B., Cai, T., Nescic Z., Spittlehouse, D.L., Livingston, N.J., 2004: Sensitivity and uncertainty of the carbon balance of a Pacific Northwest Douglas-fir forest during an El Niño/La Niña cycle. *Agric. For. Meteorol.* **123**: 201-219.
- Raupach, M.R. and Thom, A.S., 1981: Turbulence in and above plant canopies. *Ann. Rev. Fluid Mech.* **13**: 97-129.
- Redelsperger J. and Clark, T., 1990: The initiation and horizontal scale selection of convection over gently sloping terrain. *J. Atmos. Sci.* **47**, 516-541.
- Ross, J., 1975: Radiative transfer in plant communities. *Vegetation and the Atmosphere*, **Vol. 1**, J.L. Monteith ed., *Academic Press*, New York, 13-55
- Shaw, R.H., Hartog, G.D. and Neumann, H.H., 1988: Influence on foliar density and thermal stability on profiles of Reynolds stress and turbulence intensity in a deciduous forest. *Boundary-Layer Meteorol.* **45**, 391-409.
- Smagorinsky, J., 1963: General circulation experiments with the primitive equations. I. The basic experiment. *Mon. Wea. Rev.*, **91**: 99-164
- Staebler, R.M., Fitzjarrald, D.R., 2003: Observing subcanopy CO₂ advection. *Agricultural and Forest Meteorology*, **122**, 139-156.
- Stull, R.B., 1988: An introduction to boundary layer meteorology. *Kluwer Academic Publishers*, Norwell, Mass., USA
- Thom, A.S., 1971: Momentum absorption by vegetation. *Quart. J. R. Meteor. Soc.* **97**, 414-428
- Wilson, J.D., J.J. Finnigan, and M.R. Raupach, 1998: A first-order closure for disturbed plant-canopy flows, and its application to winds in a canopy on a ridge. *Quarterly J. Roy. Meteor. Soc.* **124**: 705-732
- Yamada, T, 1982: A numerical study of turbulent airflow in and above a forest canopy. *J. Meteor. Soc. Japan.* **60**, 439-454
- Yi, C., Davis, K.J., Bakwin, P.S., Berger, B.W., and Marr, L.C., 2000: Influence of advection on measurements of the net ecosystem-atmosphere exchange of CO₂ from a very tall tower. *Journal of Geophysical research*, **105**: 9991-9999
- Uchijima, Z., 1961: Bull. Nat. Inst. Agric. Sci., **Vol. A**, 243-263.